Stochastic Environmental Research and Risk Assessment (2024) 38:1163–1178
https://doi.org/10.1007/s00477-023-02622-x

ORIGINAL PAPER

Characterization of annual urban air temperature changes with special reference to the city of Modena: a comparison between regression models and a proposal for a new index to evaluate relationships between environmental variables

Isabella Morlini[1] · Sean Albertson[2,3] · Stefano Orlandini[2]

Accepted: 17 November 2023 / Published online: 11 December 2023

Abstract
It is commonly recognized that the observed increase in global mean annual air temperature is strongly related to the increase in global carbon dioxide concentration C, and that both these variables are related to global development. It remains, however, unclear the degree to which local mean annual urban air temperature T is affected by local variables such as annual precipitation depth P and urban area extent A. This study assumes that A is a proxy of local development and C is a proxy of global development and investigates the commingled effects of A, P, and C on T by using long-term annual data observed over the years 1881–2019 from the Modena Observatory in Italy. Linear relationships between T, C and A are found to be spurious since all these series have a monotonic increasing trend with time. Parametric analytic models like logistic functions are found to lack flexibility. Smoothing splines can only give insights into the strength of the relationships but not on their shape defining the functional relationship between variables. Advanced nonlinear models like generalized additive models, instead, are found to combine flexibility in a parametric form, and appear therefore to be suitable models for explaining the complex relationships between A, P, and C on T. The different models are evaluated using traditional goodness of fit statistics like R^2, AIC, BIC, and a new index of relation IR which is introduced to jointly evaluate the goodness-of-fit of relationships between variables that may either be dependent or independent.

Keywords Generalized additive models · Long-term site-based data · Urban air temperature · CO_2 concentration · Urban area extent · Precipitation · Local and global development

1 Introduction

Long-term data reported in historical archives of astronomical observatories are important to understand the long-term effects of local and global variables on urban climate (e.g., Burt 2023). Observed increase in mean annual urban air temperature T is commonly recognized to be associated with the observed increase of global carbon dioxide (CO_2) concentration C through the greenhouse effect (Jones et al. 1999; Jouzel et al. 2007; Luthi et al. 2008; Milly et al. 2008; Rehman et al. 2021). As air temperature is often measured in towns or cities displaying an urban area extent A that increases in time, some researchers have attempted to assess whether the increase of T is in part due to the increase of A (Karl et al. 1988; Kalnay and Kay 2003). At least in theory, partitioning at the land surface of net (incoming minus reflected or absorbed) shortwave and longwave radiation into sensible and latent heat fluxes is affected by land use change resulting from urbanization (Gao et al. 2019). On a broader scope, however, it remains unclear the degree to which climate local variables such as annual precipitation depth P may affect T, in addition to

✉ Isabella Morlini
isabella.morlini@unimore.it

[1] Dipartimento di Comunicazione ed Economia, Università degli Studi di Modena e Reggio Emilia, Reggio Emilia, Italy

[2] Present Address: Dipartimento di Ingegneria Enzo Ferrari, Università degli Studi di Modena e Reggio Emilia, Modena, Italy

[3] Present Address: College of Arts and Sciences, Cornell University, Ithaca, NY, USA

A and C. Many recent studies examining climate change focus on the causes and effects of local CO_2 emission (see, e.g., Wang et al. 2019; Cai and Cao 2020; Mehmood et al. 2021; Huang and Matsumoto 2021; Wang and Wang 2021) or on the relationship between temperature and precipitation (see, e.g., Regoto et al. 2021; Daramola and Xu 2022; Li et al. 2023). Several studies were performed on local effects of global warming (Zou et al. 2020; Guan et al. 2021; Skytt et al. 2021). The aim of this work is to consider the commingled effects of local climate and environmental variables such as A and P and global CO_2 concentration C on local air temperature T.

Even though there is general agreement that the annual mean temperature of Earth's surface has increased during the last century, it is obvious that this warming is quite inhomogeneous in various respects, like spatial and seasonal variability and environmental local influences. Surface modification arising from urbanization result in a tendency for urban areas to exhibit elevated temperatures relative to nonurbanized surroundings areas, a phenomenon called "urban area heat island" (Krayenhoff and Voogt 2010). Urban temperature depends on local scale and microscale processes in addition to the larger scale (e.g., synoptic) weather patterns that typically drive heat waves. In this context, it appears of relevance to study the sensitivity of surface air temperature to changes in urbanization, in addition to changes in meteorological condition, such as precipitation, and global CO_2. Understanding causation between environmental variables is particularly challenging for two reasons. First, linear models may be spurious due to the presence of similar trends in the time series. Secondly, each variable may be either dependent on other variables or one of the independent variables (Pearl 2000). For instance, changes in T may affect P and, conversely, P may cause changes in T. Granger's (1969) causality can only be tested for measuring the ability to predict the future values of a time series using prior values of the other time series, but not for measuring the ability to cause changes of a value at the same time. In the present study, the statistical relationships between annual values of T, P, A, and C are investigated through advanced statistical nonlinear models and models are compared both with traditional goodness-of-fit statistics and a new index here introduced to assess the strength of the relationships between variables considering that the same variable may be either the dependent or the independent one.

The long series of T (from 1861 to 2019) and P (from 1830 to 2019) recorded from the Modena Observatory in Italy are combined with data of A observed or reconstructed for Modena (from 1881 to 2019), and data of C observed in ice cores (from 1832 to 1958) and in Mauna Loa, Hawaii (from 1959 to 2019), so that a complete data set is obtained for the period from 1881 to 2019 (Etheridge et al. 1998; National Oceanic and Atmospheric Administration 2021). Although the data analyzed cannot provide a comprehensive global picture of how local and global developments and climatic variables affect air temperature, they can show long-term relationships between T, P, A, and C that cannot be found in any global investigation due to the scarcity of long observed (rather than simulated) time series. Local series of air temperature and precipitation depth analyzed are particularly valuable since obtained from uninterrupted daily observations collected from 01-01-1861 to 12-31-2019 at the Modena Geophysical Observatory in Italy. Metadata describing the history of the station are still available, even for the early period (Corradini 2014). Long term in situ observations (160 years per series) are not affected by important inhomogeneities caused by changes in instrumentations, station moves, different observing practices like, for instance, different formulas for calculating the minimum and the maximum or different observations time. As also highlighted by Boccolari and Malmusi (2013), the Modena time series have the advantages that sensors have been positioned in the same location, in the Eastern tower of the Ducal Palace of Modena, apart from a short period during the Second World War between 1944 and 1945. Sensors have been always controlled by at least one operator. Starting from 1985, meteorological observations are performed daily with the use of automatic equipment. A change in the hygrothermograph (an instrument used to simultaneously measure and record humidity and temperature levels in the atmosphere over time) has been done in 1869, before the starting year (1881) of the series considered in the present study. Variability is due to changes in the local and global environment and can be related to global CO_2 as well as to variations in the local development. A detailed wavelet analysis of these two series is reported in Morlini et al. (2023). The wavelet analysis shows that the scale of variation is different for temperature and precipitation and that the behavior of the temperature range values diverges from the behavior of the minimum and maximum values. The timescale of important changes in the long-term trend is, however, similar. Results also suggest that the main mode of variability is persistent through time in the series of temperature maximum, minimum and range, but not in precipitation depth. This is a clear evidence of climate change. In the present study, the local area extent A of Modena is assumed to be an indicator of local development, the global CO_2 concentration C is assumed to be an indicator of global development, and the relationship between A, P, and C on T is investigated. The paper is organized as follows: data are methods are described in Sect. 2, the statistical analyses and results are illustrated in Sect. 3, discussion and conclusions are reported in Sect. 4.

2 Materials and methods

The annual time series of mean urban air temperature T and cumulative precipitation depth P are obtained from uninterrupted daily observations collected from 1861 and from 1830, respectively, at the Geophysical Observatory of the University of Modena and Reggio Emilia (latitude 44.6474°N, longitude 10.9293°E, elevation 76.50 m asl), Modena, Italy. The series are illustrated in detail in Figs. 1 and 2. Figure 1 reports minimum, maximum, and mean values of daily temperature DT, (plots a and b), monthly temperature MT (plot c), and annual temperature AT (plot d). Solid lines indicate the mean values and gray bands indicate minimum and maximum values. To give insights into the temperature pattern, the daily values are shown in plot b for the period from 2017 to 2019. Figure 2 reports values of daily precipitation depth DPD (plots a and b), monthly precipitation depth MPD (plot c) and annual precipitation depth APD (plot d). To give insights into the precipitation pattern, the daily values are shown in plot b for the period from 2017 to 2019. Observations of urban area extent A for Modena are available for years 1881, 1940, 1961, 1971, 1981, 1998, 2000, and 2002–2019. Cubic spline interpolation is applied to obtain reconstructed values of A for the other years in the period from 1881 to 2019. Global CO_2 concentration C estimated from ice cores, from 1832 to 1958, and observed at the Mauna Loa Observatory (latitude 19.5362°N, longitude 155.5763°W, elevation 3397.00 m asl), Hawaii, from 1959, are then combined to provide the annual time series for C in the period from 1881 to 2019. The CO_2 concentration observed in Mauna Loa is used when available and the CO_2 concentration estimated from ice cores as a second possible source to complete the time series over the period 1881–2019. This is assumed to be a better choice than using available CO_2 concentration from ice cores over the

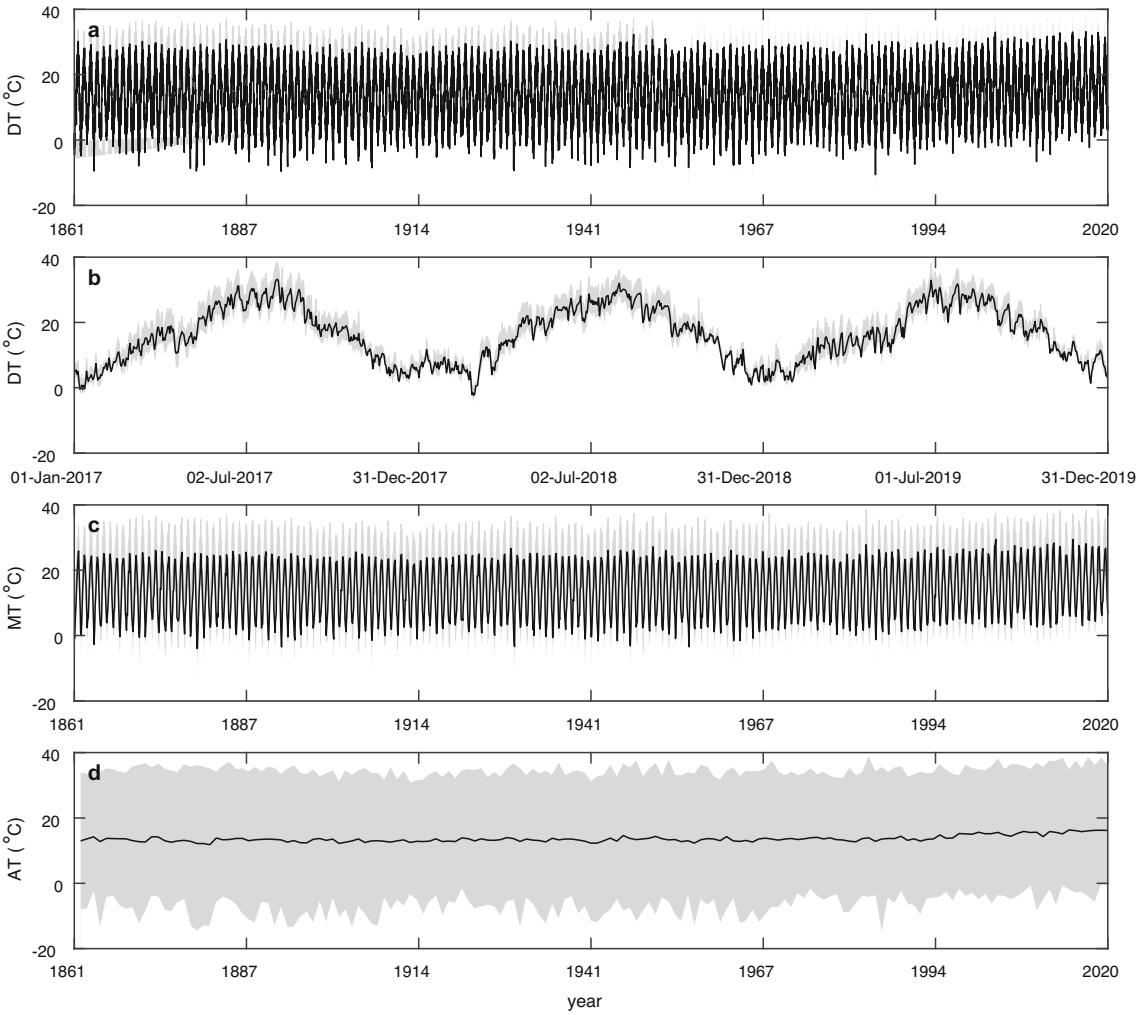

Fig. 1 Minimum, maximum, and mean values of daily temperature (plots a and b), monthly temperature (plot c) and annual temperature (plot d). Solid lines indicate the mean values and gray bands indicate minimum and maximum values

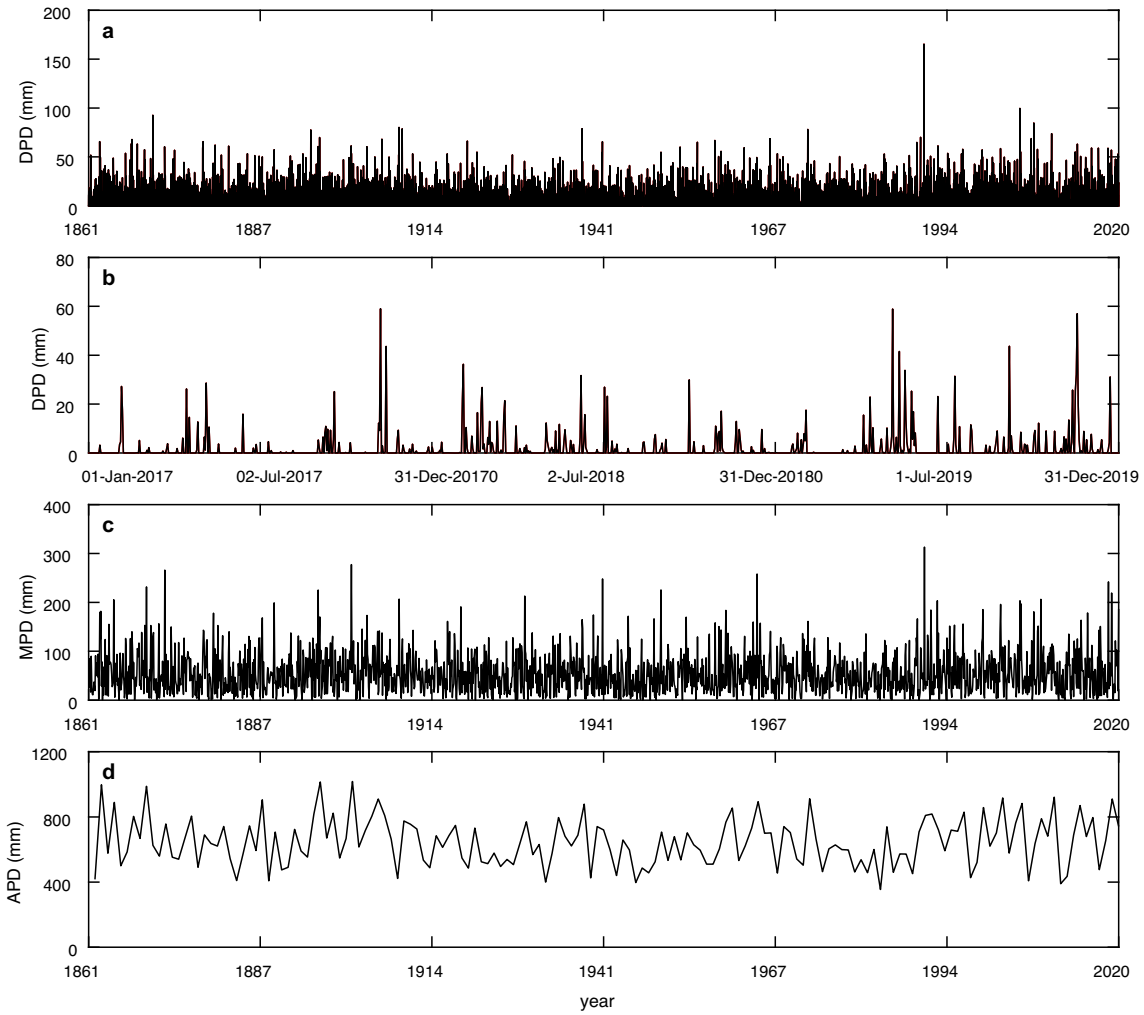

Fig. 2 Values of daily precipitation depth (plots a and b), monthly precipitation depth (plot c), and annual precipitation depth (plot d)

period 1881–2019 by neglecting the most reliable data when available.

The complete data set including 139 annual values of T, P, A and C observed or reconstructed in the period from 1881 to 2019 is shown in the scatter plot matrix reported in Fig. 3. To find symmetric and asymmetric relationships between variables, the representation of the series through a scatter plot matrix is particularly useful. Analyzing plots we can see that local temperature, local urbanization and global CO_2 are indeed pairwise related while local precipitation seems to be a variable independent from the other ones. This may be also due to the presence of extreme values (Fig. 1) and the heavy tail distribution, typical of rainfall time series (Fawcett and Walshaw 2007, 2012; Buritica and Naveau 2022). Correlation coefficient is different from zero with a significant level $\alpha = 0.001$ for T and A ($r_{TA} = 0.73$, p value < 0.0001), T and C ($r_{TC} = 0.81$, p value < 0.0001), C and A ($r_{CA} = 0.96$, p value < 0.0001), but not for P and A ($r_{PA} = 0.08$, p value $= 0.31$), P and C ($r_{PC} = 0.09$, p value < 0.36), P and T ($r_{PT} = -0.03$, p value $= 0.70$). These values suggest a strong linear relation between local temperature and local urbanization, local temperature and global CO_2 and a nearly perfect linear relation between local urbanization and global CO_2. They also suggest that precipitation depth is uncorrelated with the other variables. However, while global CO_2, local temperature and local urbanization show similar temporal patterns, local precipitation depth has a different temporal annual behavior. Even though the analysis of the trends of the different series is beyond the aim of this work, the trend impacts on the analysis of the relationships between variables in the linear case. In fact, if two variables have the same monotonic downward or upward trend, then linear correlation may be spurious.

The statistical assessment of the presence or absence of a monotonic trend, inhomogeneity, and change points, has been made by performing several nonparametric tests using XLSTAT (Addinsoft 2023). Summary results of the Mann–

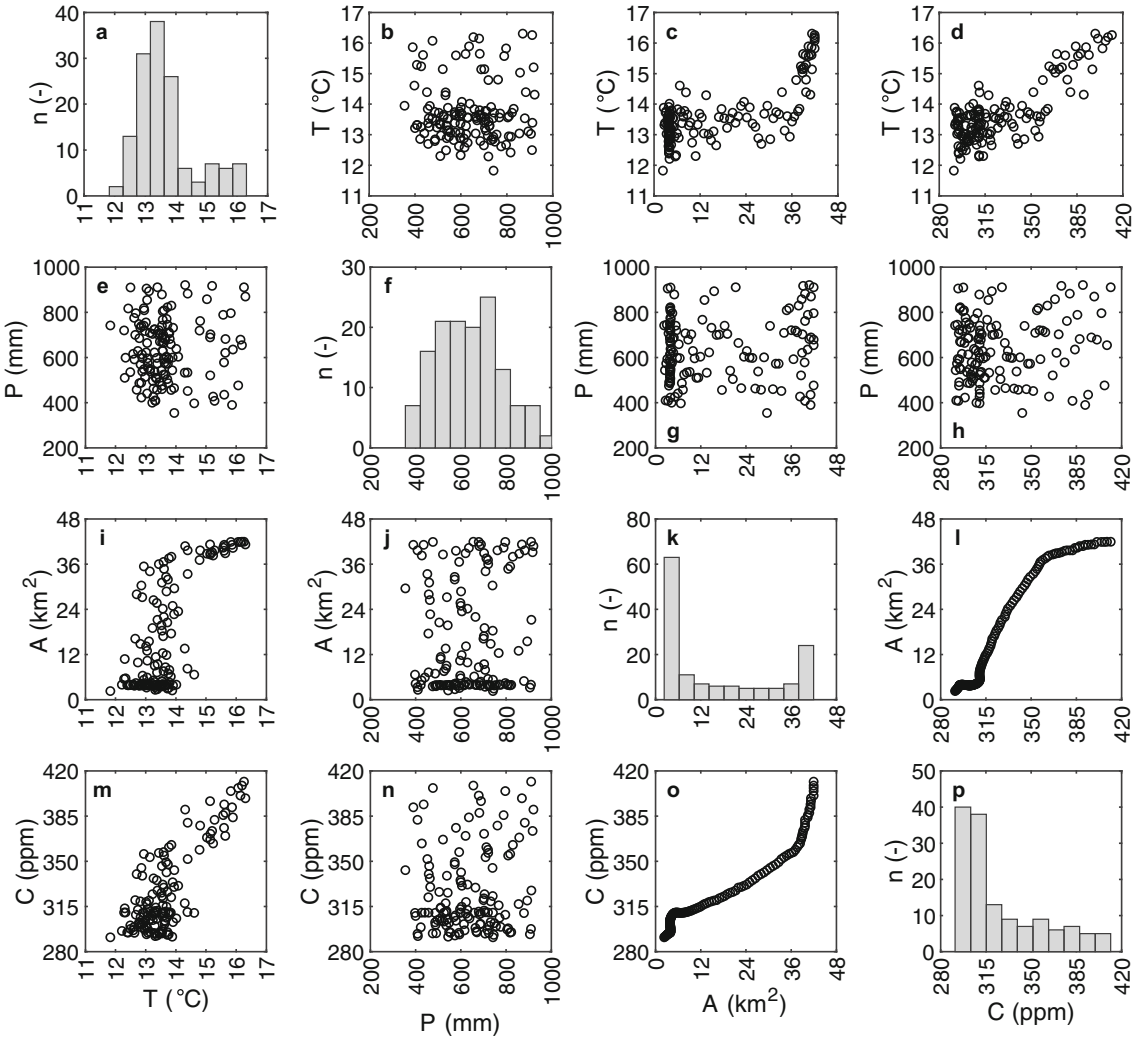

Fig. 3 Scatter plot matrix illustrating the absolute frequency distributions of variables T, P, A, and C observed from 1881 to 2019, namely the number of occurrences n over discrete intervals (diagonal plots) and pairwise relationships (plots outside the diagonal)

Table 1 Summary results of the Mann–Kendall's, von Neuman's and KPSS trend tests

Series	Mann–Kendall trend test			Von Neuman test		KPSS trend test	
	Kendall's tau	*p* value	Sen's slope	N	*p* value	Eta observed	*p* value
T (°C)	0.435	< 0.0001	0.014	0.428	< 0.0001	0.620	< 0.0001
P (mm)	0.017	0.769	0.106	1.854	0.198	0.164	0.146
A (km^2)	0.923	< 0.0001	0.324	0.001	< 0.0001	1.114	< 0.0001
C (ppm)	0.993	< 0.0001	0.631	0.001	< 0.0001	1.086	< 0.0001

Kendall (MK) test (Mann 1945; Kendal 1975; Gilbert 1987), von Neuman's test (von Neuman 1941) and KPSS test (Kwiatkowski et al. 1992) are reported in Table 1. The MK and the von Neuman tests do not require that the measurements be normally distributed or that the trend, if present, is linear. The null hypothesis is that the data come from a population with independent realizations and are identically distributed. The alternative hypothesis for the MK test is that the data follow a monotonic trend, for the von Neuman's test is that observations are not randomly distributed and are correlated. For the von Neuman's test the *p* value is computed using 10,000 Monte Carlo simulations. The Sen's slope (Sen 1968; Hipel and McLeod 1994), indicates the linear rate of change in the MK test. The KPSS test is used for testing the null hypothesis that the time series is stationary around a deterministic trend (i.e., trend-stationary) against the alternative of a unit root. Contrary to most unit root tests, the presence of a unit root

Table 2 Summary results of the Pettitt, Buishand, and SNHT change point detection tests

Series	Pettitt's test					Buishnad's test					SNHT test				
	K	*p* value	*t*	μ_1	μ_2	U	*p* value	*t*	μ_1	μ_2	*T*	*p* value	*t*	μ_1	μ_2
T (°C)	3086	< 0.0001	1965	13.2	14.4	44.9	< 0.0001	1993	13.3	15.3	97.51	< 0.0001	1996	13.3	15.5
P (mm)	932	0.468	1988	641	641	11.2	0.270	1988	641	641	5.21	0.329	1988	641	641
A (km^2)	4830	< 0.0001	1949	4.3	28.3	62.5	< 0.0001	1965	5.7	33.2	119.9	< 0.0001	1971	6.6	35.1
C (ppm)	4830	< 0.0001	1949	301	350	57.5	< 0.0001	1970	305	364	109.2	< 0.0001	1981	308	373

is not the null hypothesis but the alternative. Additionally, in the KPSS test, the absence of a unit root is not a proof of stationarity but, by design, of trend-stationarity. This is an important distinction since it is possible for a time series to be non-stationary, have no unit root yet be trend stationary. All tests show departures from the first-order stationarity in the *T*, *A*, *C* series and, conversely, do not detect a significant trend in *P*. This last result agrees with the absence of a univocal direction of trend (or lack thereof) in annual total precipitation depth in Italy shown in the study of Caporali et al. (2021). The MK test also indicates that the trend in *T*, *A* and *C* is positive.

Summary results of the Pettitt's (Pettitt 1979; Verstraeten et al. 2006), Buishand's (Buishand 1982, 1984), and SNHT (Alexandersson 1986) tests for a shift in the central tendency are reported in Table 2. In these tests, the null hypothesis is that the observations follow one or more distributions that have the same location parameter μ (no change), against the alternative that a change point *t* exists, and the time series have a location parameter μ_1 before the change point *t* and a location parameter μ_2 after the change point. The *p* value is computed using 10,000 Monte Carlo simulations.

These three tests also support the hypothesis of non-stationarity of *T*, *A*, *C* and first-order stationarity of the *P* series. Even though the change points identified by the tests are different, they however agree in rejecting the null hypothesis of a constant location parameter over time in all series except the *P* one. It is interesting noting that, for *A* and *C*, the change points identified by the Pettitt's test are identical and differ only 5 years in the Buishand's test and 10 years in the SNHT test. This finding supports the hypothesis of a very similar pattern of the local urbanization in Modena and the global CO_2 and the necessity to use nonlinear bivariate relationships to avoid spurious results (Yule 1926; Granger et al. 2001). It can also be noticed that the performed tests do not reveal abrupt changes when the CO_2 concentration observed in Mauna Loa (1881–1958) is introduced in preference to CO_2 concentration estimated from ice cores (1959–2019). In the presented study, tests for change point detection are primarily carried out to provide a measure of the robustness of the results from previous three tests, namely Mann–Kendall, Von Neuman, and KPSS trend tests (e.g., Ferguson and Villarini 2021). Since all tests agree in rejecting the null hypothesis for *T*, *A* and *C* and in rejecting the null hypothesis for *P*, there is consistency in the results. To assess a time interval for the change point in the three inhomogeneous series, it must be noted that, although the Buishand, Pettitt and SNHT tests for change point detection have in common the characteristic of estimating simultaneously the presence of abrupt changes and linear trend, they however differ in terms of distributional assumptions. The Buishand test is particularly suitable to detect breaks near the beginning and the end of a series relatively easily, whereas the Pettitt test is more sensitive to breaks in the middle of a time series (Hawkins 1977). The Buishand and the SNHT tests assume that the values are normally distributed, but the Pettitt test does not. The reason that the Pettitt test does not require such an assumption is that this test is based on the ranks of the elements of a series rather than on the values themselves. The ranking approach of the Pettitt test also implies that it is less sensitive to outliers than the other tests. It is common to have different estimated break points when applying all tests, especially in climatic or hydrological time series and especially in long time series (see, e.g., Ferguson and Villarini 2021; Winjngaard et al. 2003). With respect to the Buishand test, the change points detected by the SNHT test agree within three years in the *T* time series, within six years in the *A* time series and within eleven years in the *C* time series. These are reasonable ranges suggesting that a break in *P* fell around 1993–1996, in *A* within the period 1965–1971, and in *C* within the period 1970–1981 (Winjngaard et al. 2003). Results confirm that the tests are not robust to the distributional assumptions. Examining the location parameters before and after the change points, it can be observed for the Buishand and SNHT tests that the distance between the two values is higher with respect to the same distance calculated for the Pettitt test, and this is reasonably because Pettit test considers ranks rather than values.

Spuriousness of the correlation coefficients is also confirmed by the analysis of the correlation coefficients computed for first order differences ΔT, ΔA, ΔC, ΔP. If two

variables are correlated, their changes are also correlated. This is for instance a foundation in cointegration studies, and the Engel-Granger approach, where if a long-run relationship between two variables exists, there is also a short-term relationship. The correlation coefficient computed for first order differences is different from zero with a significant level $\alpha = 0.001$ for ΔT and ΔP ($r_{TP} = -0.32$, p value < 0.0001), ΔA and ΔC ($r_{AC} = 0.30$, p value $= 0.000$) but not for the other couples of variables. These results suggest the existence of a direct short-term relationship between A and C and an inverse short-term linear relationship between P and T.

2.1 Asymmetric relationships with temperature as dependent variable

2.1.1 Analysis with a single explicative variable

We first evaluate and compare asymmetric pairwise relationships considering the temperature as the dependent variable and, in turn, the local urbanization, the global CO_2 and the local precipitation depth as the explicative variable. For studying these pairwise asymmetric relationships, we use both parametric and nonparametric models, namely logistic function and smoothing splines, the first one conveying information in the values of the estimated parameters, the second ones being more flexible. Let $\{x_i, y_i, I = 1, \ldots, n\}$ be a set of observations, modeled by the relation $y_i = f(x_i) + e_i$, where e_i are independent zero mean random variables. Let $\widehat{y}_i = f(x_i)$ be the predicted values. The 4-parameter logistic function is defined as the following function

$$f(x_i) = d + (a - d)/\left[1 + (x_i/c)^b\right] \quad (1)$$

minimizing the sum of squares error SSE = . Parameter a is the minimum asymptote, b is the Hill's slope, c is the inflection point and d is the maximum asymptote. The routine L4P available for Matlab is used to fit the function. We compare logistic models with a different explicative variable considering the complement to one of coefficient of determination R^2. Exploiting the property that the average value $\overline{y}$ of observations y_i ($I = 1, \ldots, n$) is equal to the average value $\overline{y}$ of predicted values $\widehat{y}_i$ ($I = 1, \ldots, n$), we use the following normalized sum of squares error (NSE), giving the percentage of variability of the dependent variable not explained by the relationship with the predictor variable:

$$NSE = \sum_{i=1}^{n}(y_i - \widehat{y}_i)^2 / \sum_{i=1}^{n}(y_i - \overline{y})^2 = 1 - R^2 \quad (2)$$

Cubic smoothing splines (Reinsch 1967; Wahba 1990; De Bor 2001) encompass a family of widely used nonlinear semiparametric flexible functions. They are the functions $f(x_i)$, over the class of twice differentiable functions, minimizing the quantity.

$$S\sum_{i=1}^{n}\left(\frac{\widehat{y}_i - y_i}{w_i}\right)^2 + (1 - S)\int (f''(x_i))^2 dx, \quad (3)$$

where S is a smoothing factor in [0 1] and w_i are weights controlling the extent of smoothing of each point. With the smoothing factor S ranging from 0 to 1, the fitting function range from the least squares straight-line fit to the natural cubic interpolant to the given data. We implement splines with $S = 0.2, 0.4, 0.6, 0.8, 1.0$. and with $w_i = 1$ for $I = 1, \ldots, n$. We compare models with the same explicative variables and with a different explicative variable considering the Aikake Information Criterion (AIC) and the Bayesian Information Criterion (BIC) (Burnham et al. 2011; Findely 1991; McQuarrie and Tsai 1998; Stoica and Selen 2004; Schwarz 1978). These criteria estimate the prediction error and thereby the relative quality of statistical model fitting for a given set of data. They are founded on information theory and estimate the relative amount of information lost by a given model: the less information a model loses, the higher is the fitting of that model. In estimating the amount of information lost, AIC and BIC deal with the trade-off between the goodness of fit and the complexity of the model, given by the number of parameters. In terms of the sum of squares error, AIC and BIC can be written as

$$\mathrm{AIC} = n\ln\left(\sum_{i=1}^{n}(y_i - \widehat{y}_i)^2/n\right) + 2k \quad (4)$$

and

$$\mathrm{BIC} = n\ln\left(\sum_{i=1}^{n}(y_i - \widehat{y}_i)^2/n\right) + k\ln(n) \quad (5)$$

where k is the number of parameters of the model. The penalty term $k\ln(n)$ in BIC is larger than the penalty term in AIC, $2k$, for $n > 7$ (Stoica and Selen 2004). Differently from the sum of squares error, these errors are used in flexible models to prevent overfitting.

2.1.2 Multivariate analysis

We use generalized additive models (GAM) to study T as a function of P, A and C. Considering m explicative variables $X_1, X_2, \ldots, X_m$, equation describing GAM is

$$g(y_i) = f_0 + f_1(x_{1i}) + \ldots + f_m(x_{mi}), \quad (6)$$

where $g(\cdot)$ is a link function, f_0 is a constant, f_i, $I = 1, \ldots, m$, are shape functions. GAM are particularly suitable to describe complex nonlinear relationships between observed geophysical quantities since they can capture the signal and filter the noise in observed data (Hastie and Tibshirani 1986, 1990). Moreover, in GAM we may separate and compare the contribution of each explicative variable and

see the effect of each predictor on the prediction. The routine "fitrgam" available in Matlab 2011b is used in the present study (Lou et al. 2012, 2013) and contributions to GAM predictions are determined by using the routine "plotlocaleffects." Since the link function $g(\cdot)$ is set equal to the identity link function, the GAM used can more specifically be denoted as additive models (Lou et al. 2012). GAM implemented in Matlab incorporate non-parametric shape functions like trees and bagged trees with a large, undetermined number of parameters. For this reason, AIC and BIC cannot be computed for these models. Models are fitted with the gradient boosting algorithm (Friedman 2001, 2002) and overfitting is controlled through cross validation. Exploiting the property that the average value of observations y_i ($I = 1, \ldots, n$) is equal to the average value of predicted values $\widehat{y}_i$ ($I = 1, \ldots, n$) to compare different models we use the NSE defined in (2).

2.2 Pairwise asymmetric relationships with unknown dependent variable

We propose in this section a new data driven technique for evaluating the strength of the asymmetric relationship between two variables when both variables may either be the dependent or the independent variable. The peculiarity of most of the atmospheric variables and human-driven related variables is that it is not clear, a priori, the direction of causality. For instance, air temperature may cause changes in precipitation depth and, conversely, precipitation depth may cause change in air temperature. Moreover, local urbanization may cause changes in the global environment if the global environment may cause change in local urbanization. This peculiarity especially occurs when we are not considering lagged variables since we are rather interested in yearly values.

We use generalized additive models (GAM) to study the relations $\widehat{y}_i = f(x_i)$ with $Y = T, P, A, C$ and $X = T, P, A, C$. For each model, we compute the NSE, which can be used to compare the fitting also among models with a different dependent variable Y. We compute the NSE for each pair of variables, indicating by $(K \mid Z)$ the model in which K is the dependent variable and Z the explicative variable and by $(Z \mid K)$ the model in which Z is the dependent variable and K the explicative variable. Note that the NSE for the model $(Z \mid Z)$ or $(K \mid K)$ may not be exactly equal to zero, as nonlinear functions used in GAM may not fit exactly linear functions. To evaluate the strength of the relationship between K and Z, supposing the direction of causality is not known a priori, we introduce the following index of relationship IR:

$$\mathrm{IR}(K,Z) = 1 + \lceil \mathrm{NSE}(K|K)\mathrm{NSE}(Z|Z) - \mathrm{NSE}(K|Z)\mathrm{NSE}(Z|K) \rceil \quad (7)$$

The index as the following properties:

1. NSE($K \mid K$) NSE ($Z \mid Z$) – NSE($K \mid Z$) NSE($Z \mid K$) is the determinant of the 2 × 2 matrix having rows [NSE($K \mid K$), NSE($K \mid Z$)] and [NSE($Z \mid K$), NSE ($Z \mid Z$)], that is
$$IR(K,Z) = 1 + |NSE(K|K)NSE(K|Z)NSE(Z|K)NSE(Z|Z)|$$
.
2. IR is a symmetric index, i.e., IR (Z, K) = IR (K,Z).
3. IR ranges from 0 to 1: when IR = 0 there is no relationship between K and Z, when IR = 1, there is the strongest interrelationship between K and Z that can be described by the model used.
4. IR (K,Z) = 1 – [$R^2(K \mid K)$ $R^2(Z \mid Z)$ – $R^2(K \mid Z)$ $R^2(Z \mid K)$] when the average value of observations y_i ($I = 1, \ldots, n$) is equal to the average of values $\widehat{y}_i$ ($i = 1, \ldots, n$) predicted by the model.

Just like the determinant of the variance–covariance matrix of a data set is referred to as the generalized variance of the data set (Anderson 2003; Wilks 1932) since the determinant generally gives the magnitude of a matrix transformation and, in case of variances and covariances, it gives the measure of magnitude of how much the variables vary with each other, the determinant of the matrix having rows [NSE($K \mid K$), NSE ($K \mid Z$)] and [NSE($Z \mid K$), NSE ($Z \mid Z$)] gives the measure of magnitude of how much the models make errors with each other. Differently from the variance–covariance matrix, the matrix having rows [NSE($K \mid K$), NSE ($K \mid Z$)] and [NSE($Z \mid K$), NSE ($Z \mid Z$)] is not symmetric when nonlinear models are evaluated and the determinant is zero or negative.

In case of comparing, an IR for a couple of variables (K, Z) bigger than the IR for another couple of variables indicates that the first two variables have a stronger causal relationship than the other two. We can consider IR a normalized, symmetric, comparable index based on asymmetric relationship analysis. Since symmetric analyses are unsuitable to determine causation and causation is defined a priori in asymmetric (regression) analysis, both the possible dependencies of K on Z and of Z on K are used to define IR (K,Z) so that it can be used when causation between K and Z is a priori unknown.

3 Analysis and results

3.1 Smoothing splines and logistic functions

Time series of mean annual air temperature T observed in Modena from 1881 to 2019 is plotted with time series urban area extent A of Modena in Fig. 4a, and with time series of CO_2 concentration C observed in ice cores and in Mauna Loa in Fig. 4b. Figure 4c and d show values of T estimated by some nonlinear functions of A and C,

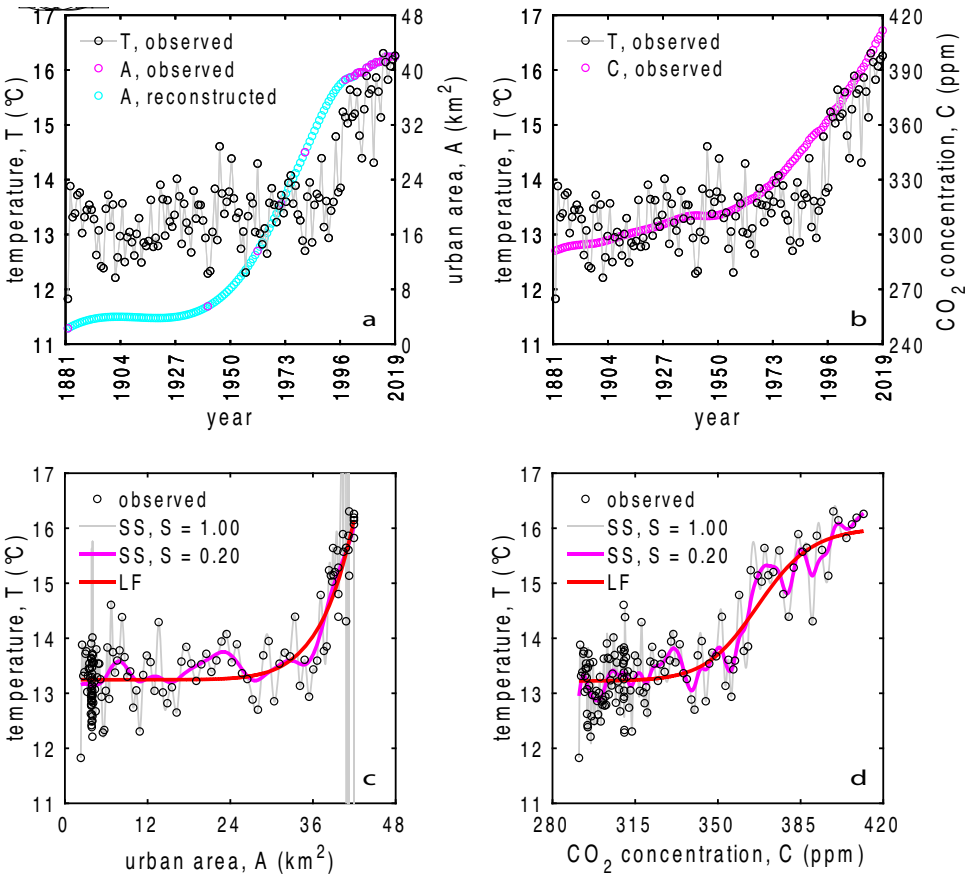

Fig. 4 Time series of T and A (plot a), T and C (plot b), estimated values of T considering A (plot c) and C (plot d) as dependent variable using smoothing splines (SS) with parameters 1 and 0.2 and the 4-parameter logistic function (LF)

Table 3 Estimated parameters of the 4-parameter logistic function and NSE

	Explicative variable		
	A	*C*	*P*
a	13.25 °C	13.22 °C	14.83 °C
b	8.50 °C	33.44 °C	0.32 °C
c	113.7 km^2	367.3 ppm	425 mm
d	13,950 °C	16.01 °C	12.64 °C
NSE	0.273	0.0.275	0.998

respectively. In Fig. 4 are reported cubic smoothing splines with $S = 1.0$ and $S = 0.2$ and the 4-parameter logistic function LF. Table 3 reports the NSE error (2) for the estimated LF functions (1) and the values of the parameters (results of the 5-parameters logistic functions are not reported since they are very similar for the values of the parameter and for the goodness of fit).

The LF function has good and very similar fit when *C* and *A* are used as explicative variables, and a very poor fit when *P* is used as predictor. This indicates that *A* and *C* convey the same information in predicting *T* and have the same strength of relationship with *T,* while *P* seems unrelated to *T*. The *C*-*T* curve is steeper than the *A*-*T* curve. While the estimated minimum temperature for a zero urban area extent and a zero CO_2 global emission is the same (13 °C) the maximum temperature estimated for an infinite value of *A* is 13,950 °C and the maximum temperature estimated for an infinite value of *C* is 16.01 °C. The inflection point, that is the value of the dependent variable for which the curve change direction or the value for which the estimated temperature is nearly half of the maximum value), is 113.7 km^2 for *A* and 367.3 ppm for *C*. Even though the estimated values of some of the parameters are implausible, due to the lack of flexibility of this function, we may get some insights into the comparison of the *C*-*T* and the *A*-*T* relationships. The Hill's slope suggests that the first one is steeper than the second one. The maximum asymptote suggests that, while temperature continues increasing with increases in the urban area extent, it stops increasing after a certain value of CO_2. Moreover, while half of the maximum possible value has been reached in relation to *C*, it has not yet been reached in relation to *A*.

Table 4 reports AIC and BIC for the smoothing splines. As expected, the interpolating splines (SS with $S = 1$) overfit the data. The best fit for each dependent variable is given by smoothing splines with parameter $S = 0.2$. Comparing information criteria, we see that variable *A* is a

Table 4 Akaike Information Criterion (AIC) and Bayesian Information Criterion (BIC) of Smoothing Splines (SS)

Fitting function	Independent variable					
	A		*C*		*P*	
	AIC	BIC	AIC	BIC	AIC	BIC
SS with $S = 1.0$	639	1027	639	1027	653	1061
SS with $S = 0.8$	426	501	486	694	582	884
SS with $S = 0.6$	416	475	466	598	561	841
SS with $S = 0.4$	409	458	451	561	548	802
SS with $S = 0.2$	402	441	435	523	528	751

slightly better predictor than *C*. *P*, as expected, is found to be the worst predictor. Since the functions are nonparametric, we cannot get insights into the relationships between variables, but we can only compare the goodness of fit given the strength of the relationships. Splines support results obtained by the LF function, indicating that *P* is unrelated to *T* and that *A* and *C* convey the same information in predicting *T*.

Possible relationships between the examined variables and the North Atlantic Oscillation (NAO) teleconnection index are also investigated in the present study. The NAO index is a measure of the atmospheric pressure difference between the Icelandic Low and the Azores High in the North Atlantic region. It is a climate index that may influence weather patterns in the Northern Hemisphere, particularly in Europe and North America. The NAO can be in a positive or negative phase, affecting the strength and position of the jet stream, which in turn influences weather patterns (Barnston and Livezey 1987). It is found, however, that the NAO index is not related with *T* and with *P*. In addition, using the NAO index instead of *P* does not give improved predictions of *T* (Appendix 1).

3.2 Generalized additive models

Multivariate relationships are evaluated implementing GAM for predicting *T* as a function of sets of two variables and as a function of all three predictors. Models are compared considering the NSE error defined in (2). Predicted and observed *T* values, as well as the NSE errors, are shown in Fig. 5: plot a reports results with $X = [A, C]$, plot b with $X = [P, C]$, plot c with $X = [P, A]$, and plot d with $X = [P, A, C]$.

For models with three predictors, separate contributions to the predicted *T* are evaluated and reported in Fig. 6. Equation (6) can be written as $T = f_0 + f_1(P) + f_2(A) + f_3(C)$, where $f_0 = 13.667$ °C, $f_1(P)$ ranges from − 1.229 to 0.573 °C, $f_2(A)$ ranges from − 0.836 to 1.281 °C, and $f_3(C)$ ranges from − 0.686 to 1.113 °C.

Over the entire observation period 1881–2019, the constant value f_0 is equal to 13.667 °C and the mean values (MV) of $f_1(P)$, $f_2(A)$ and $f_3(C)$ are equal to zero. The MV of $f_1(P)$, $f_2(A)$ and $f_3(C)$ are found to vary from − 0.018 to 0.011 °C (+ 0.029 °C), from − 0.166 to 0.378 °C (+ 0.544 °C), and from − 0.343 to 0.408 °C (+ 0.751 °C), respectively, when the 50-year periods of time 1881–1930 and 1970–2019 are compared. Results show that the most accurate couple of predictors is $X = [P, C]$. Slightly less accurate predictions are obtained with $X = [P, A]$, indicating that *A* and *C* convey essentially the same information content. The most accurate predictions of *T* are obtained when all the three predictors $X = [P, A, C]$ are used, confirming the expected greater flexibility of the GAM with three predictor variables. A relatively minor improvement is obtained when $X = [P, A, C]$ is used in preference to $X = [P, C]$ with respect to the improvement in prediction accuracy obtained by using $X = [P, C]$ in preference to $X = [A, C]$. Therefore, although *P* is poorly related to other variables when considered singly, it contributes to improve predictions when considered in combination with other predictor variables related to local or global development. Since *T* and P display different, relatively unsmoothed paths with respect to *A* and *C, P* may therefore convey additional information for the prediction of *T* with respect to the one conveyed by *A* and *C*. Analysis of GAM predictions of *T* obtained when $X = [P, A, C]$ confirms that over the 139-year period of time from 1881 to 2019 fluctuations of *T* around the mean value $f_0 = 13.667$ °C are more importantly due to predictors *A* and *C* than to predictor *P*. Variations over time of these contributions indicate that urban area extent *A* has played a slightly less important role than *C* in the last 50 years.

GAM predictions obtained for any couple of variables are shown in the scatter plot matrix of Fig. 7. In each plot, the related NSE is reported. Diagonal plots show the prediction of a variable given the same variable as the predictor. As outlined before, the NSE may not be exactly equal to zero in these cases since nonlinear function may not fit exactly a perfect linear relation. Table 5 reports the IR defined in Eq. (7). Results show that the most accurate predictions of *T* are obtained by using *C* or *A* as a single predictor, indifferently. They also surprisingly indicate that there is a perfect nonlinear relationship when considering *A* as a function of *C* (NSE = 0) and an almost perfect relationship when considering *C* as a function of *A* (NSE = 0.002). There is a perfect nonlinear relationship when considering that both *C* and *A* can be the dependent or the independent variable ($IR = 1$).

This suggests the hypothesis that these variables are both driven by a third causative factor such as, for instance, economic growth. As urban area extent *A* of Modena was measured independently from CO_2 concentration

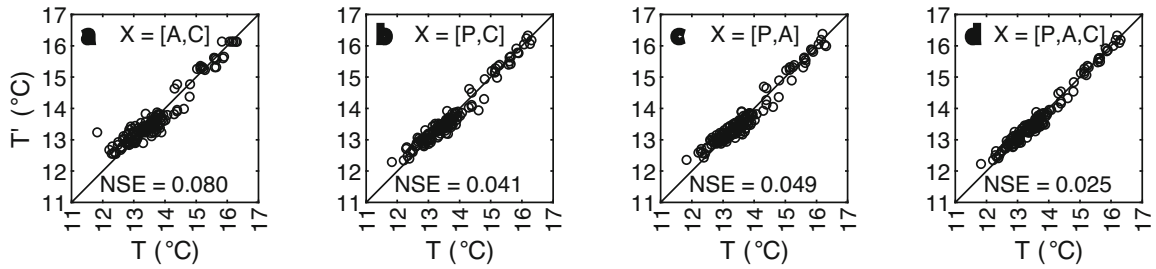

Fig. 5 Observed and predicted values of T by Generalized Additive Models with $X = [A, C]$ (plot a), $X = [P, C]$ (plot b), $X = [P, A]$ (plot c), and $X = [P, A, C]$ (plot d). Plots also report the normalized squared error of the models

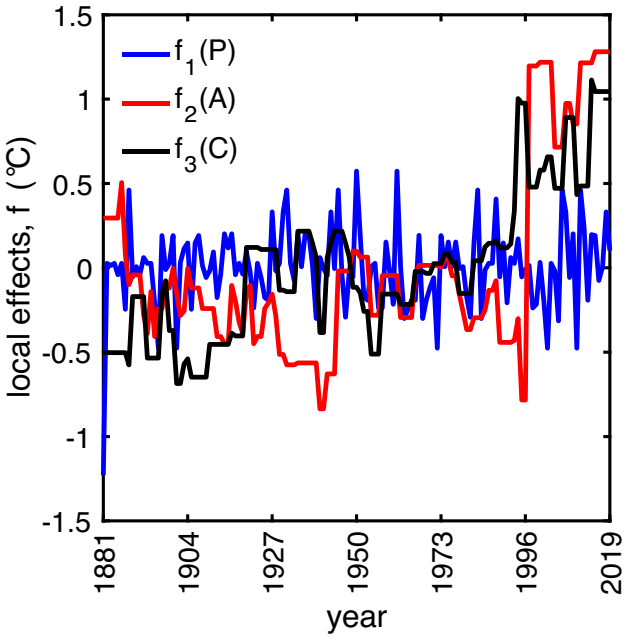

Fig. 6 Separate contributions to GAM predictions

C observed in ice cores and in Mauna Loa, and no physical reason is found for a cause-and-effect relationship between A and C, it may be hypothesized that the relationship between A and C is connected to a third causative factor such as economic grow or demographic grow. The local development that drove the increase of urban area extent of Modena appears to have marched in step with the global development that drove the rise in atmospheric CO_2 concentration. Obtained values of the index of relationship are compatible with this hypothesis. However, we outline that it is not possible from this time series analysis to apportion the observed temperature increase between the causal pathways of global greenhouse forcing and local urbanization forcing on the surface energy balance.

The analysis confirms that P alone is not a good predictor of the other variables. However, considering that P may affect T, and T may affect P, there is a quite strong relationship between the two variables (IR = 0.761). The same result holds considering P and C. When evaluating P as dependent variable, we see that dependence on A and C is weak: the NSE are 0.486 and 0.439, respectively. This result seems interesting since it points out that, while temperature is strongly linked to local and global effects of urbanization, annual precipitation depth in Modena seems to be unrelated to these effects.

4 Discussion and conclusions

The aim of this study was twofold. The first aim was to investigate the relationships among observed increase in mean annual urban air temperature in Modena, Italy, increase in global CO_2 concentration, local precipitation depth and local urban area extent, over long time series. The second aim was to find a new data-driven approach to data modeling and a new index of relationship considering that an environmental variable may be either dependent on other variables or one of the independent variables, and the direction of causation is often unknown. The analysis presented in this study reveals that both local urbanization and global CO_2 concentration are important predictors compared to precipitation, and that urbanization has played a slightly less important role than CO_2 concentration in the last 50 years (Sect. 3.2). While there is no evident physical connection between local urbanization and global CO_2 concentration to explain similar temporal patterns, the process of economic development had direct implications on both urban area extent measured in Modena and CO_2 concentration observed in global data sets (Sect. 3.1; Figs. 4, 5, 6, and 7; Table 3, 4, and 5). It appears that the local development driving urban area extent occurred along the same temporal pattern as the global development driving global CO_2 concentration (Sect. 2; Figs. 3 and 7; Table 1 and 2). This should not be seen as a total surprise, as western economic development proceeded in parallel across much of Europe and North America, and this overall western development was the major contributor to global anthropogenic greenhouse gas emissions of the twentieth century. While local air temperature, global CO_2 and local urbanization are strictly interconnected, local precipitation

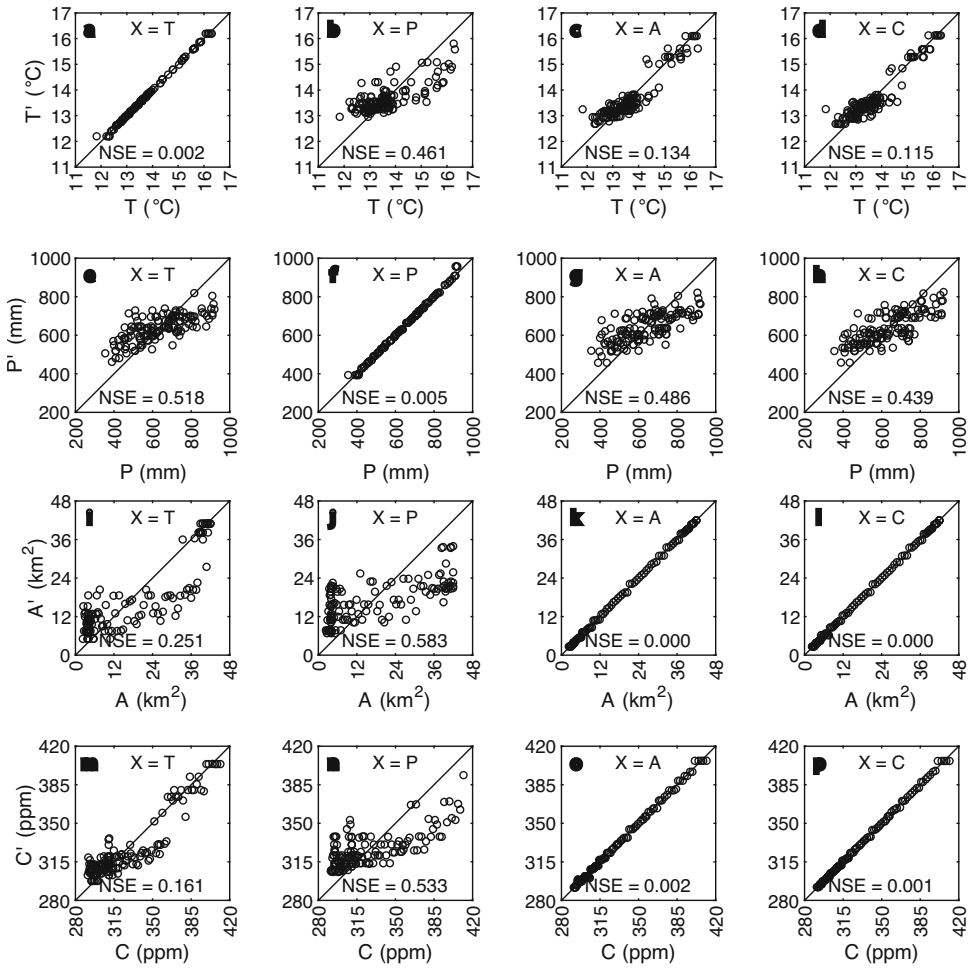

Fig. 7 Scatter plot matrix of observed and estimated values of T (plots a, b, c, d), of P (plots e, f, g, h), of A (plots I, j, k, l), and of C (plots m, n, o, p) with GAM with the single predictor variable T (plots a, e, I, m), P (plots b, f, j, n), A (plots c, g, k, o) and C (plots d, h, l, p)

Table 5 IR values for GAM univariate relationships

Variable *Y*	Variable *X*			
	T	*P*	*A*	*C*
T	1.000	0.761	0.966	0.982
P	0.761	1.000	0.716	0.766
A	0.966	0.716	1.000	1.000
C	0.982	0.766	1.000	1.000

depth seems to be unrelated to local urbanization and global CO_2 and it seems an important predictor of local air temperature only when used together with the other considered variables (Figs. 3, 5, and 7; Table 4).

The analysis carried out reveals that linear relationships between urban air temperature, urban area extent and global CO_2 concentration may be affected by spuriousness since all series have a significant monotonic and positive trend and relationships should be evaluated with nonlinear models (Tables 1 and 2). Among nonlinear models, analytic model like the 4-parameter logistic function has a good fit but the parameters show that it is unsuitable for future predictions, since the maximum temperature estimated for an infinite value of local urbanization is 13,950 °C (the estimated curve is too steep out of the domain of the observed values in Fig. 4) and, conversely, the maximum temperature estimated for an infinite value of *C* is 16.01 °C (the curve is almost constant out of the domain of the observed values in Fig. 4). A possible explanation of this different pattern of the two logistic functions is that while air temperature *T* and global CO_2 concentration *C* show consistent annual increases in the last decade (from 2011 to 2019), local urban area extent *A* shows a slight annual increase from 2001 to 2015 and remains nearly constant from 2015 to 2019. As shown in Fig. 4c, the logistic function captures the increase in *T* due to quite constant values in *A* in the last decade by assuming a very sharp shape, while it captures increases in *T* due to relative higher increases in *C*, by assuming a smother shape (Fig. 4d). The discrepancy between the estimated *T*-*A* and *T*-*C* relationships may be due to the different pattern in the last decade, showing high increases in *T* related to small

Table 6 *P* values of different homogeneity tests

Test	Mann–Kendall	Von Neuman	KPSS	Pettitt	Buishand	SNHT
p value	0.098	0.514	0.027	0.112	0.065	0.153

Table 7 Correlation coefficients and related *p* values (in brackets)

Variable	T (°C)	P (mm)	NAO
T (°C)	1 (0)	0.039 (0.751)	0.139 (0.250)
P (mm)	0.039 (0.751)	1 (0)	− 0.012 (0.922)
NAO	0.139 (0.250)	− 0.012 (0.922)	1 (0)

increases or constant values in A and moderate increases in T due to relatively higher increases in C. Smoothing splines with a proper degree of smoothness ($S = 0.2$ or $S = 0.4$) show a good fit. Information criteria indexes indicate that more flexible smoothing splines ($S > 0.4$) do not distinguish signal and noise in the estimated relationship and overfit the observed data (Table 4). Even with a proper degree of smoothness, however, smoothing splines do not give insights into the relationships between environmental variables since they are nonparametric models. Unlike other nonlinear models, GAM seems to be flexible enough to capture the relationships among variables and can be considered as parametric models. Indeed, the contribution of each explicative variable can be evaluated and compared by analyzing the coefficient of each additive function (Fig. 6). Results show that global CO_2 and precipitation depth, and the couple of predictor local urbanization and precipitation depth, have the same accuracy in predicting local temperature. Therefore, local urbanization and global CO_2 seem to convey essentially the same information content in predicting local temperature. The most accurate prediction of temperature is obtained when all the three considered predictors are used. This indicates that although local precipitation is poorly related to other variables when considered singly, it contributes to improve predictions when considered in combination with other predictors (Figs. 5 and 6). The analysis of single contributions f_0, $f_1(P)$, $f_2(A)$, and f_3(C) to local temperature $T = f_0 + f_1(P) + f_2(A) + f_3$(C) reported in Fig. 6 reveals an increase of + 0.029 °C in the MV of $f_1(P)$, an increase of + 0.544 °C in the MV of $f_2(A)$, and an increase of + 0.751 °C in the MV of f_3(C) when the 50-year periods of time 1881–1930 and 1970–2019 are compared, indicating that the role of CO_2 concentration C has been increasingly important.

To analyze the causal effect of a variable on another it is considered that in climate modeling the direction of causality is often reciprocal when not considering lagged variables. For instance, air temperature causes changes in precipitation depth and precipitation depth causes changes in air temperature. We have therefore introduced a new interrelationship index considering the fit of the model in which the first variable is the dependent one (and the second variable is the independent one) and the fit of the model in which the first variable is the independent one (and the second variable is the dependent one). The index is normalized and does not depend on the scale of measurement of the variables (Eq. 7). The index shows, for instance, that even though precipitation depth alone is not a good predictor for the temperature, considering that the temperature may be a predictor for the precipitation depth, there is a quite strong relationship between the two variables (Table 5). Regarding the methodology, future work is needed to analyze the behavior of the index of relationship in simulated data sets, and to apply this index to other environmental data. Future work is needed to examine how extensive this tight coupling between time series of local urban area extent and global CO_2 concentration is across other western cities. A special effort is also needed to further investigate the relative influence of urbanization and CO_2 concentration along mechanistic lines of inquiry.

Appendix 1

Considering annual values of the NAO teleconnection index, from 1950 to 2019, the statistical assessment of the presence or absence of a monotonic trend, inhomogeneity and change points, has been made by performing several nonparametric and parametric tests, using XLSTAT (Addinsoft 2023). *P* values of the different tests are reported in Table 6.

At the 1% level, all tests agree in accepting the null hypothesis that the annual values are independent, and the series is homogeneous. Correlations with the other climatic series of P and T are then likely to be nonspurious. Correlation coefficients and *p* values are reported in Table 7.

The correlation between the NAO index and precipitation P, and the correlation between the NAO index and temperature T are clearly not significant. To further investigate the influence of the NAO index on the local temperature T and compare the nonlinear relationship between T and NAO with the nonlinear relationship between T and C and T and A, different smoothing splines and the 4-parameter logistic function are estimated. In Fig. 8, cubic smoothing splines with $S = 1.0$ and $S = 0.2$ and the 4-parameter logistic function LF are reported.

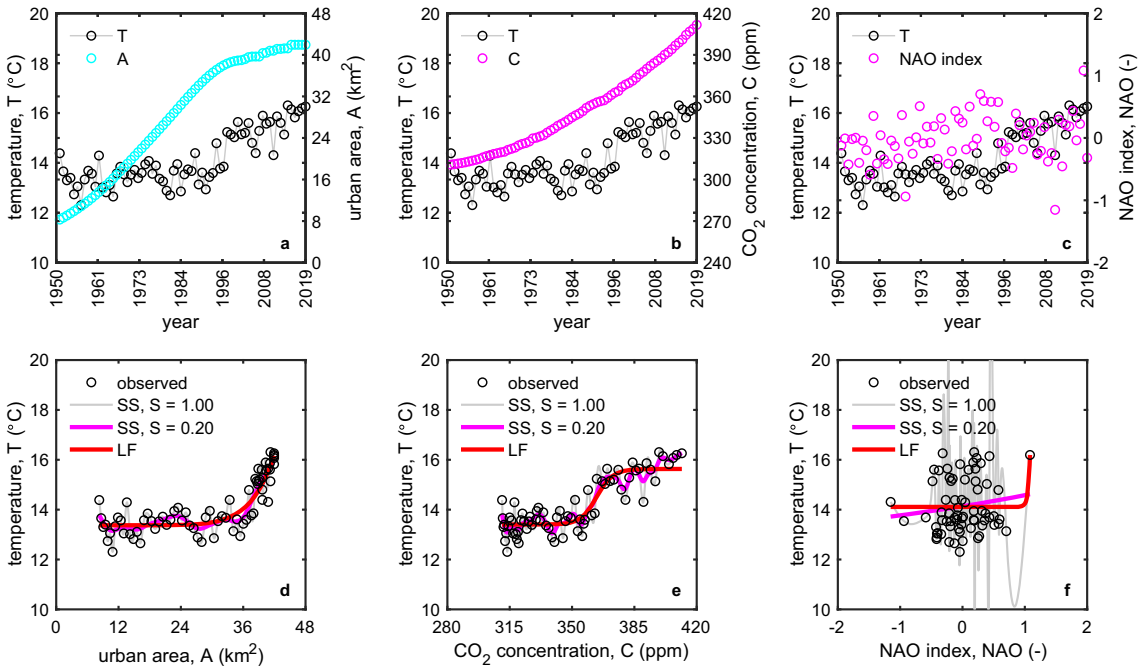

Fig. 8 Time series of T and A (plot a), T and C (plot b), T and NAO (plot c), estimated values of T considering A (plot d) and C (plot e) and NAO (plot f) as dependent variable using smoothing splines (SS) with parameters 1.00 and 0.20 and the 4-parameter logistic function (LF)

Table 8 NSE errors

Function	A	C	NAO
SS with $S = 1.0$	0.026	0.000	0.016
SS with $S = 0.8$	0.112	0.039	0.976
SS with $S = 0.6$	0.126	0.060	0.974
SS with $S = 0.4$	0.139	0.083	0.977
SS with $S = 0.2$	0.157	0.110	0.979
4-parameter logistic	0.212	0.216	0.947

Table 8 reports the NSE error (2) for smoothing splines. Clearly, smoothing splines with $S = 1.0$ overfit the data, while all the other estimated smoothing splines have similar AIC and BIC values (not reported) and can be selected as models with a proper degree of smoothness.

Both the graphical representation of the estimated functions and the values of the NSE indicate that local urbanization A and the global CO_2 concentration C are more related to local temperature T than the NAO index and are better predictors of temperature changes in the last 70 years. In conclusion, results suggest that neither local precipitation P nor the NAO index seem to be related to the local temperature T. This may be because local geographical features may modify the impact of the NAO index on precipitation and temperature in specific areas.

Acknowledgements Air temperature and precipitation time series of Modena were provided by the Geophysical Observatory of the University of Modena and Reggio Emilia, Modena, Italy. Luca Lombroso is greatly acknowledged for providing specific comments and feedback on these data. The research reported in the present paper was supported by Fondazione Cassa di Risparmio di Modena through the grant 2018-0093, by the University of Modena and Reggio Emilia through the grant FAR 2020 Mission Oriented, and by the European Union NextGenerationEU/NRRP, Mission 4 Component 2 Investment 1.5, Call 3277 (12/30/2021), Award 0001052 (06/23/2022), under the project ECS00000033 "Ecosystem for Sustainable Transition in Emilia-Romagna," Spoke 6 "Ecological Transition Based on HPC and Data Technology." The authors thank the anonymous reviewers for comments that led to improvement in the manuscript.

Author contributions All authors contributed to the study conception and design. Material preparation, data collection and analysis were performed by Isabella Morlini, Sean Albertson and Stefano Orlandini. The first draft of the manuscript was written by Isabella Morlini and Stefano Orlandini and all authors commented on previous versions of the manuscript. All authors read and approved the final manuscript.

Funding The authors have no relevant financial or non-financial interests to disclose.

Data availability Data sets used in this study are available at https://doi.org/10.1594/PANGAEA.938740.

Declarations

Conflict of interest The authors declare no conflicts of interest relevant to this study.

References

Addinsoft (2023) XLSTAT Statistical and data analysis solutions. New York, USA. https://www.xlstat.com

Alexandersson H (1986) A homogeneity test applied to precipitation data. J Climatol 6:661–675
Anderson TW (2003) An introduction to multivariate statistical analysis. Wiley Series in Probability and Statistics
Barnston AG, Livezey RE (1987) Classification, seasonality and persistence of low-frequency atmospheric circulation patterns. Mon Wea Rev 115:1083–1126
Boccolari MA, Malmusi S (2013) Changes in temperature and precipitation extremes observed in Modena, Italy. Atmos Res 122:16–31
Buritica G, Naveau P (2022) Stable sums to infer high return levels of multivariate rainfall time series. Environmetrics. https://doi.org/10.1002/env.2782
Burnham KP, Anderson DR, Huyvaert KP (2011) AIC model selection and multimodel inference in behavioural ecology. Behav Ecol Sociobiol 65:23–35. https://doi.org/10.1007/s00265-010-1029-6
Buishand TA (1982) Some methods for testing the homogeneity of rainfall records. J Hydrol 58:11–27
Buishand TA (1984) Tests for detecting a shift in the mean of hydrological time series. J Hydrol 73:51–69
Burt SD (2023) A twice-daily barometric pressure record from Durham observatory in north-east England, 1843–1960. Geosci Data J 10(1):3–17. https://doi.org/10.1002/gdj3.135
Cai Z, Liu Q, Cao S (2020) Real estate supports rapid development of China's urbanization. Land Use Policy 95:104582
Caporali E, Lompi M, Pacetti T, Chiarello V, Fatichi S (2021) A review of studies on observed precipitation trends in Italy. Int J Climatol 41:E1–E25
Corradini E (2014) From the geophysical-meteorological Observatory of Modena to the Italian network of observatories. In: Proceedings of the 12th conference of the international committee of ICOM for University Museums and Collections (UMAC), Singapore, 10–12 Oct, 2012. https://doi.org/10.18452/8741
Daramola MT, Xu M (2022) Recent changes in global dryland temperature and precipitation. Int J Climatol 42(2):1267–1282. https://doi.org/10.1002/joc.7301
De Boor C (2001) A practical guide to splines. Springer
Etheridge DM, Steele LP, Langenfelds RL, Francey RJ (1998) Historical CO_2 record derived from the Law Dome DE08 and DE08-2 ice cores. https://cdiac.ess-dive.lbl.gov/trends/co2/lawdome-data.html
Fawcett L, Walshaw D (2007) Improved estimation for temporally clustered extremes. Environmetrics 18:173–188
Fawcett L, Walshaw D (2012) Estimating return levels from serially dependent extremes. Environmetrics 23:272–283
Ferguson CR, Villarini G (2021) Detecting inhomogeneities in the Twentieth Century Reanalysis over the central United States. J Geophys Res 117: D05123. https://doi.org/10.1029/2011JD016988
Findley DF (1991) Counterexamples to parsimony and BIC. Ann Inst Stat Math 43(3):505–514. https://doi.org/10.1007/BF00053369
Friedman J (2001) Greedy function approximation: a gradient boosting machine. Ann Stat 29:1189–1232
Friedman J (2002) Stochastic gradient boosting. Comput Stat Data Anal 38:367–378
Gao Z, Hou Y, Chen W (2019) Enhanced sensitivity of the urban heat island effect to summer temperatures induced by urban expansion. Environ Res Lett 14(9):094005. https://doi.org/10.1088/1748-9326/ab2740
Gilbert RO (1987) Statistical methods for environmental pollution monitoring. Wiley, New York
Granger CWJ (1969) Investigating causal relations by econometric models and cross-spectral methods. Econometrica 37:424–438
Granger CWJ, Ghysels E, Swanson NR, Watson MW (2001) Essays in econometrics: collected papers of Clive W. J. Granger. Cambridge University Press
Guan Y, Lu H, Jiang Y, Tian P, Qiu L, Pellikka P, Heiskanen J (2021) Changes in global climate heterogeneity under the 21st century global warming. Ecol Indic 130:108075
Hastie T, Tibshirani R (1986) Generalized additive models (with discussion). Stat Sci 1:297–318
Hastie T, Tibshirani R (1990) Generalized additive models. Chapman & Hall/CRC
Hawkins M (1977) Testing a sequence of observations for a shift in location. J Am Stat Assoc 72:180–186
Hipel KW, McLeod AI (1994) Time series modelling of water resources and environmental systems. Elsevier Science, New York
Huang Y, Matsumoto KI (2021) Drivers of the change in carbon dioxide emissions under the progress of urbanization in 30 provinces in China: a decomposition analysis. J Clean Prod 322:129000
Jones PD, New M, Parker DE, MartinS RIG (1999) Surface air temperature and its changes over the past 150 years. Rev Geophys 37(2):173–199. https://doi.org/10.1029/1999RG900002
Jouzel J, Masson-Delmotte V, Cattani O, Dreyfus G, Falourd S, Hoffmann G, Minster B, Nouet J, Barnola JM, Chappellaz J, Fischer H, Gallet JC, Johnsen S, Leuenberger M, Loulergue L, Luethi D, Oerter H, Parrenin F, Raisbeck G, Raynaud D, Schilt A, Schwander J, Selmo E, Souchez R, Spahni R, Stauffer B, Steffensen JP, Stenni B, Stocker TF, Tison JL, Wernerm M, Wolff E (2007) Orbital and millennial Antarctic climate variability over the past 800,000 years. Science 317(5839):793–797. https://doi.org/10.1126/science.1141038
Kalnay E, Kay M (2003) Impact of urbanization and land-use change on climate. Nature 423:528–531. https://doi.org/10.1038/nature01675
Karl TR, Diaz HF, Kukla G (1988) Urbanization: its detection and effect in the United States climate record. J Clim 1(11):1099–1123
Kendal MG (1975) Rank correlation methods, 4th edn. Charles Griffin, London
Krayenhoff ES, Voogt JA (2010) Impacts of urban albedo increase on local air temperature at daily–annual time scales: model results and synthesis of previous works. J Appl Meteorol Climatol 49:1634–1648
Kwiatkowski D, Phillips PCB, Schmidt P, Shin Y (1992) Testing the null hypothesis of stationarity against the alternative of a unit root. J Econometrics 54(1–3):159–178
Li J, Xie H, Li J, Yang G, Xie Y, Wang J, Zhou C, Zou S (2023) Influences of anthropogenic acids on carbonate weathering and CO_2 sink in an agricultural karst wetland (South China). Ecol Indic 150:110192
Lou Y, Caruana R, Gehrke J (2012) Intelligible models for classification and regression. In: Proceedings of the 18th ACM SIGKDD international conference on knowledge discovery and data mining (KDD '12), Beijing, China. ACM Press, pp 150–158
Lou Y, Caruana R, Gehrke J, Hooker G (2013) Accurate Intelligible Models with Pairwise Interactions. Proceedings of the 19th ACM SIGKDD International Conference on Knowledge Discovery and Data Mining (KDD '13) Chicago, Illinois, USA, ACM Press: 623–631
Luthi D, Floch ML, Bereiter B, Blunier T, Barnola JM, Siegenthaler U, Raynaud D, Jouzel J, Fischer H, Kawamura K, Stocker TF (2008) High resolution carbon dioxide concentration record 650,000–800,000 years before present. Nature 453:379–382. https://doi.org/10.1038/nature06949
Mann HB (1945) Non-parametric tests against trend. Econometrica 13:163–171

McQuarrie ADR, Tsai CL (1998) Regression and time series model selection. World Scientific
Mehmood U, Tariq S, Haq ZU (2021) Effects of population structure on CO_2 emissions in South Asian countries: evidence from panel estimation. Environ Sci Pollut Res 28:66858–66863
Milly PCD, Betancourt J, Falkenmark M, Hirsch RM, Kundzewicz ZW, Lettenmaier DP, Stouffer RJ (2008) Stationary is dead: whither water management? Science 319:573–574. https://doi.org/10.1126/science.1151915
Morlini I, Franco-Villoria M, Orlandini S (2023) Modelling local climate change using site-based data. Environ Ecol Stat 30(2):205–232
Oceanic and Atmospheric Administration (2021) Trends in atmospheric carbon dioxide. https://gml.noaa.gov/ccgg/trends/
Pearl J (2000) Causality: models, reasoning, and inference. Cambridge University Press
Pettitt AN (1979) A non-parametric approach to the change point problem. J R Stat Soc: Ser C Appl Stat 28:126–135
Regoto P, Dereczynski C, Chou SC, Bazzanella AC (2021) Observed changes in air temperature and precipitation extremes over Brazil. Int J Climatol 41(11):5125–5142
Rehman A, Ma H, Ahmad M, Irfan M, Traore O, Chandio AA (2021) Toward environmental sustainability: devolving the influence of carbon dioxide emission to population growth, climate change, forestry, livestock and crops production in Pakistan. Ecol Indic 125:107460
Reinsch CH (1967) Smoothing by Spline Functions. Numer Math 10(3):177–183. https://doi.org/10.1007/BF02162161
Sen PK (1968) Estimates of the regression coefficient based on Kendall's tau. J Am Stat Assoc 63:1379–1389
Stoica P, Selen Y (2004) Model-order selection: a review of information criterion rules. IEEE Signal Process Mag. https://doi.org/10.1109/MSP.2004.1311138
Schwarz GE (1978) Estimating the dimension of a model. Ann Stat 6(2):461–464. https://doi.org/10.1214/aos/1176344136
Skytt T, Nielsen SN, Jonsson B (2021) Global warming potential and absolute global temperature change potential from carbon dioxide and methane fluxes as indicators of regional sustainability—A case study of Jämtland, Sweden. Ecol Indic 130:108075
Verstraeten G, Poesen J, Demaree G, Salles C (2006) Long-term (105 years) variability in rain erosivity as derived from 10-min rainfall depth data for Ukkel (Brussels, Belgium): implications for assessing soil erosion rates. J Geophys Res 111:D22109
Von Neumann J (1941) Distribution of the ratio of the mean square successive difference to the variance. Ann Math Stat 12:367–395
Wahba G (1990) Spline models for observational data. SIAM, Philadelphia
Wang Q, Wang L (2021) The nonlinear effects of population aging, industrial structure, and urbanization on carbon emissions: a panel threshold regression analysis of 137 countries. J Clean Prod 287:125381
Wang J, Wu Y, Zhao Y, He S, Dong Z, Bo W (2019) The population structural transition effect on rising per capita CO_2 emissions: evidence from China. Clim Policy 19(10):1250–1269
Wilks SS (1932) Certain generalizations in the analysis of variance. Biometrika 24:471–494
Winjngaard JB, Klein Tank AMG, Konnen GP (2003) Homogeneity of 20th century European daily temperature and precipitation series. Int J Climatol 23:679–692
Yule GU (1926) Why do we sometimes get nonsense-correlations between time-series? A study in sampling and the nature of time-series. J R Stat Soc 89(1):1–63. https://doi.org/10.2307/2341482
Zou F, Li H, Hu Q (2020) Responses of vegetation greening and land surface temperature variations to global warming on the Qinghai-Tibetan Plateau, 2001–2016. Ecol Indic 119:106867